Conductivity Analysis for High-Resolution EEG

Sergei I. Turovets
NeuroInformatics Center
5294 University of Oregon
Eugene, OR 97403, USA
sergei@cs.uoregon.edu

Pieter Poolman
Electrical Geodesics, Inc.
Eugene, OR 97403, USA
ppoolman@egi.com

Adnan Salman
NeuroInformatics Center
5294 University of Oregon
Eugene, OR 97403, USA
adnan@cs.uoregon.edu

Allen D. Malony
NeuroInformatics Center
5294 University of Oregon
Eugene, OR 97403, USA
malony@cs.uoregon.edu

Don M. Tucker
Electrical Geodesics, Inc.
Eugene, OR 97403, USA
dtucker@egi.com

Abstract

We describe a technique for noninvasive conductivity estimation of the human head tissues in vivo. It is based on the bounded electrical impedance tomography (bEIT) measurements procedure and realistically shaped high-resolution finite difference model (FDM) of the human head geometry composed from the subject specific co-registered CT and MRI. The first experimental results with two subjects demonstrate feasibility of such technology.

1. Introduction

Electroencephalography (EEG) is an indispensable neurological diagnostic tool in terms of the fast time scale, portability and cost efficiency. Improved spatial resolution of EEG measures would greatly benefit multiple clinical and research applications, including stroke, epilepsy and cognitive studies. The recent advances in dense-array electrode application have made EEG brain imaging for both rapid application and long-term monitoring feasible [1]. It has been shown that reliable inverse solutions can be obtained and dense-array sampling (128, 256 and 512 channels) on the scalp can be projected back to the cortex, providing a unique opportunity for monitoring brain activity both in space and time. However, the spatial accuracy of EEG will remain limited because i) mostly simplistic models of the human head (like multi-shell spheres) are commonly used in the inverse procedure of back-to-cortex projection, and ii) the regional conductivities of the human head tissues are largely unknown. Several imaging modalities have been proposed so far to quantitatively measure the electrical conductivity of tissue non-invasively, but none of them is free from some limitations and shortcomings. Magnetoacoustic Hall effect imaging [2] relies on propagation of ultrasound into the tissue, and is not quantitative. Magnetic resonance current density imaging [3] requires applying rather high level of external currents to make the produced magnetic field contrast visible to MRI. The electrical conductivity tensor of tissue can be quantitatively inferred from the water self-diffusion tensor as measured by diffusion tensor magnetic resonance imaging (DTI) [4]. It can be successful in extracting anisotropic conductivities of the brain tissue, but more problematic with respect to bone (skull) tissues where the water content is much smaller.

The lack of accurate skull conductivity (most resistive tissue) is particularly problematic given the developmental variations in the human skull from infancy through adolescence. Without an accurate forward model of the skull (specifying the volume conduction from cortex to scalp) even advanced inverse efforts cannot achieve precision with EEG data as the error of source localization, due to the conductivity uncertainty, may reach a few centimeters [5].

Several authors addressed this problem by using noninvasive electrical impedance tomography (EIT) approach. In EIT, harmless currents are injected into the body, and the potential field created by volume conduction of this current through body tissues is

978-0-7695-3118-2/08 $25.00 © 2008 IEEE
DOI 10.1109/BMEI.2008.358

measured. From the potential field and the known position of the injected current, properties of the body tissue can be inferred. Although this method has been researched for many years, it has not been successfully applied to medical problems [6]. A major factor in the poor adoption of EIT is that it was initially conceived as an imaging method. However, traditional EIT is generally assumed to exhibit low spatial resolution in the presence of resistive interfaces like skull tissues, particularly at the low frequencies of physiological interest.

The problem of skull conductivity can be properly addressed *in vivo* within the framework of bounded (or parameterized) EIT applied to a subject prior to EEG measurements. The word "parameterized" is key, as it means just a few unknown parameters must be resolved during the inverse search. This is much less ambitious than the classic EIT, which seeks imaging of the subject interior in terms of conductivity on a pixel-to-pixel basis. Mathematically (and in practical computational terms), a parameterized EIT solution is much more reliable, stable and easier to find [7]. Parameterization of the realistic geometry of the human head can be accomplished by means of segmentation of MRI/CT scans into several tissues and anatomical parcellation of the skull into its constituent parts. The whole head conductivity map can then be represented by compartments with unknown piecewise constant conductivities and known boundaries. Several previous studies have been reported by other authors who parameterized the problem to solve for a small number of conductivity parameters using nonlinear inverse methods and assuming that the internal geometry of the head is already known. Oostendorp et al. [8], and Van Burik and Peters [9] showed in a three-layer boundary element (BEM) head model that it appears possible to determine the scalp/brain ratio. Gonçalves et al. [10] also applied spherical and a three-layer BEM to fit their EIT measurements for six subjects. However, since in such models skull thickness and conductivity are interchangeable to some extent, more accurate geometry representation is needed. We note here that BEM models have problems in dealing with skull inhomogeneities and anisotropies [11] and, in fact, are topologically equivalent to the spherical models. Recently we have shown in our group that by using the parameterized EIT procedure and realistically shaped high-resolution finite difference models (FDM) of the human head, it was possible to extract three and four tissues conductivities [12,13]with the multi-start downhill simplex algorithm [14], and up to 13 conductivities with the simulated annealing algorithm [15] with good accuracy in simulations with synthetic data. A similar approach was used by Hoekema et al. [16] in the conductivity measurements of skull parts temporarily removed during epilepsy surgery; however, fitting for only one unknown parameter was performed.

It is apparent that solving the conductivity information problem is a prerequisite to source localization. It can be performed, in essence, using the same EEG measurement equipment, with the small difference that a few electrode pairs must be used to inject safe levels of current, while the rest of the electrodes are used to record the potentials of the injected current. There is one important difference from the classic EIT: for the present project it is necessary to work in the range of low EEG frequencies (1-100 Hz), where effects of the electrode polarization (contact impedance) [17] may become significant and require a complete electrode computational model [18]. As a result of such an inverse procedure, we still will have just estimates (not exact) of conductivities of the constituent regional tissues, but we assume that applying a realistic head geometry, with very high accuracy, will balance this uncertainty with other EEG error contributions. The ultimate criteria, however, would be the accuracy of EEG source localization, determined with account of different possible error contributions, like measurement noise or systematic bias of the particular computational inverse procedure. Such contributions could originate also from local structural skull inhomogeneities and anisotropies [11], [19] and appropriate balance between them is still to be investigated in a systematic way.

In this paper we report the results of our first experiments performed with human subjects. Because the same EEG spectral range and electrodes are used for bounded EIT (bEIT) as for measuring EEG, the bEIT procedure provides an efficient, low-cost specification of the electrical volume conduction through head tissues. With dense-array bEIT measured as routinely as testing scalp electrode impedance, we can realize the promise of recent biophysics simulations suggesting that, with accurate correction for head tissue conductivity, EEG provides spatial resolution of brain activity that is equal to or better than magnetoencephalography (MEG) [20].

2. Methods and Materials

2.1 Hardware and Data acquisition

For our bEIT studies, we employed the existing NetAmps 300 EEG amplifier (manufactured by Electrical Geodesics, Inc.) and an isolated current generator. The NetAmps 300 platform synchronously digitizes 256 analog channels at 20 kHz and 24 bits, and uses a field-programmable gate array (FPGA) to collate and transfer data in IEEE 1394 (Firewire)

format to a computer. The NetAmps 300 platform uses "sigma-delta" type A-to-D converters, achieving high linearity, accuracy and resolution at low cost, so that each detector can have a dedicated A-to-D converter, without the need for high-speed multiplexing of different detector signals onto a single higher-speed A-to-D converter.

The current source is battery-powered and isolated from the amplifier circuitry. The waveform of the injected current is sensed across a resistor with known value and in series with the impedance load containing the head and injector/sink electrodes. Current injection parameters, e.g. source/sink electrodes, frequency, and amperage are set via a software interface. Initial experimental results pointed to current leakage somewhere in the current injection setup. Circuit analysis and subsequent testing indicated that the combination of T-filters on the NetAmps 300 front-end and a shared common ground plane between the amplifier and current source was the root cause. Therefore, in our latest design, the current source is battery-powered and isolated from the NetAmps 300 circuitry in order to eliminate leakage current through the shared common ground plane in the amplifier. Through trial and error we settled on a Howland-type design. Advantages of this topology over other designs include its small number of components, a single active device and the ability to adjust output resistance [21].

For each subject, a properly sized 128 (or 256) -channel HydroCel Geodesic Sensor Net (HCGSN) is applied and the electrode positions are measured with the Geodesic Photogrammetry System (GPS) [22]. Together with the extracted EEG topography/injector data, the head MRI/CT geometry (including electrode position) forms the input to our FDM modeling process.

During the bEIT data acquisition, sinusoidal current injection, at frequencies ranging from 1 Hz to 8 kHz, is performed for specified electrode pairs via the current source, while acquiring impressed EEG data with the NetAmps 300 data collection system. The current level is chosen to maximize the data quality. The aim is to inject current levels that that will provide good signals for data analysis without saturating the amplifier. The level of injected current (1-60 μA) is well below the accepted health and safety levels. The frequency range of the injected current is chosen to comply with the Nyquist limit of the 20 kHz sampling rate of the EEG amplifier. It is noted that high injection frequencies (several kHz) may lead to alternative and intractable current paths due to the impact of stray capacitances in the amplifier, leads, etc. This issue will be addressed in future in more detail.

2.2 Signal processing

Extraction of the amplitude and phase from the induced bEIT potentials is based on a software implementation of locked-in detection [23,24]. A lock-in detector takes as input a periodic reference signal and a noisy system signal, and extracts only that part of the system signal that matches the reference signal in frequency. The lock-in detector yields remarkable sensitivity at the locked-in frequency, and is capable of discarding the impact of offset errors, 1/f noise, etc. efficiently. In short, the building blocks of the lock-in detector consist of a phase-adjustable reference signal, multiplication, low-pass filtering, and time averaging.

For the purposes of our current injector, the reference signal is sensed across a series resistor in the current loop. It is therefore impractical to attempt to phase shift the reference signal in order to zero out the unknown system signal phase. We have shown that in the absence of a phase-adjustable reference signal, a high-fidelity software lock-in detector can be assembled by integrating a band-pass filter, zero-crossing counter, and time-series regression, e.g. via a Fourier transform. The working principle of this modified lock-in detection is based on minimizing the impact of non-DFT frequency components in reference and system signals, and ensuring that the reference frequency coincides with a DFT frequency. Given multiple-frequency EIT data, the lock-in detector can also be used to extract amplitudes and phase angles of individual frequency components from a mixed sinusoid signal. The data flow through the modified lock-in detector is described in more details in our concurrent paper at CISP 2008 [24].

2.3 Computational Framework

There are several vital components for accomplishing the conductivity estimation task: 1) develop an accurate computational model; 2) acquire a high-quality experimental data set, and 3) match the simulation with experiment with a posteriori corrections, if needed, to the modeling and experimental procedures to reach convergence. In practice this is an iterative process. To develop an accurate computational model of electrical field distribution in a human head with high geometrical precision provided by MRI/CT scans (1 mm), we have employed a Finite Difference (FD) 3D numerical solver [25] and parallelize it in a multi-cluster environment [12], [26]. With an appropriate inverse solver we have been able to mimic the whole bEIT cycle of conductivity estimation using the synthetic data corrupted with realistic noise levels. It has been proven that at least with up 10% Gaussian noise level,

the conductivity extraction for synthetic data is still viable.

In our preliminary work [12], to solve the nonlinear optimization problem, we employed the downhill simplex method of Nelder and Mead. Our observation was that simplex search performs well when the number of parameters is few (three or four parameters), however we found it reaches the practicality limits with more unknowns and fails to converge frequently. More than that, to avoid the local minima in the simplex search, we used a statistical approach. The inverse procedure was repeated for hundreds of randomly generated sets of conductivity guesses from appropriate physiological intervals, and then the solutions closest to the global minimum solution were selected using a simple error threshold criteria and results were averaged. With the higher geometry resolution and further differentiation of skull and soft tissue parts, a more powerful technique is required. For instance, beyond single digit numbers of search parameters and 1 mm MRI/CT resolution, the simplex computation quickly becomes impractical. To pursue higher dimensionality, it was clear we must replace the simplex method used in our earlier work. We chose the advanced simulated annealing algorithm which is a Monte-Carlo global minimization technique. It has been shown to be more robust for optimization across complex multi-variate search spaces. This algorithm has allowed us to extend the conductivity modeling to study the impact of skull inhomogeneities on the conductivity modeling [15].

The most heavy computational processing on posteriori conductivity extractions in the inverse procedure has been performed at the University of Oregon Neuroinformatics Center, where a three-cluster (IBM p650; IBM p690; IBM BladeServer) high performance parallel computing system, dedicated to analysis of human EEG and MEG data, has been constructed. In what follows, the work done to accomplish these tasks and the final results are described.

3. Results

BEIT measurements have been performed so far for 4 adult subjects, two males, Subjects 11 and 12 (Caucasian and Asian) and two females, Subjects 14 and 15 (both Caucasian). The male subjects already have had high-resolution MRI and CT 3D head scans, while the female subjects have had only MRI scans. Table 1 summarizes processed information for Subjects 11 and 12 and retrieved tissue conductivities.

The preliminary developed data acquisition protocol and system have been extensively tested in a series of longitudinal experiments with Subj. 11. The initial hope that the alpha hardware prototype can provide both current injection and acquisition of return potentials from the dense sensor array of the Geodesic Sensor Net had not been confirmed beforehand. Initially there was no good match between experimental and simulated potential topography for impressed EEG. We had to iterate through a few of cycles of the hardware revisions, to eliminate possible current leakages through the EEG amplifier circuitry, and signal processing amendments and testing until we obtained a working hardware prototype, data preprocessing scheme and measurement protocol. Besides hardware and signal acquisition flaws, there was also a problem of leaky channels in the dense-array net which distorted the observation of the real impressed EEG topography significantly. Two reasons for electrical leakage in bad leads (channels) have been identified. The first reason was due to occasional moisture in the intra-electrode volume between the shielding and wire core (of the coaxial leads) and resulted in electrical coupling through the amplifier common to active injecting electrodes. The second, and more frequent in EEG measurements, reason was due to saline bridges, especially around the active electrode, which resulted in dispersed current injection pattern. It should be noted that the probability of bad channels in a dense array of electrodes may be higher than in arrays with lower electrodes count unless special measures of precaution are taken. We have found that frequent lead shortcut tests and the careful handling of nets in the process of saline agitation, disinfection and storage prevents moisture from leaking into the space under lead shields. After having experimented with several types of nets and electrolytes for a while we concluded that nets with no shields and gel instead of saline provide the best performance. This system is still to be further tested, tuned and optimized. An important tool in understanding and interpreting the experimental results on-line is a graphical user interface (GUI) to control the experiment, and real-time processing of the signal. We also pre-calculated a priori impressed topographies

Table 1. The Human Subject Experiments Results, Conductivity in S/m

Subj./site	*MRI/CT*	*Age/Gend.*	*Skull*	*Scalp*	*Brain*
11/26-90	Yes	40/M	.020	.46	.23
11/46-109			.010		
12/26-2	Yes	38/M	.011		
12/15-72			.016	.52	.36

on a generic atlas head models with the injection/sink pair configurations used afterwards in experiments.

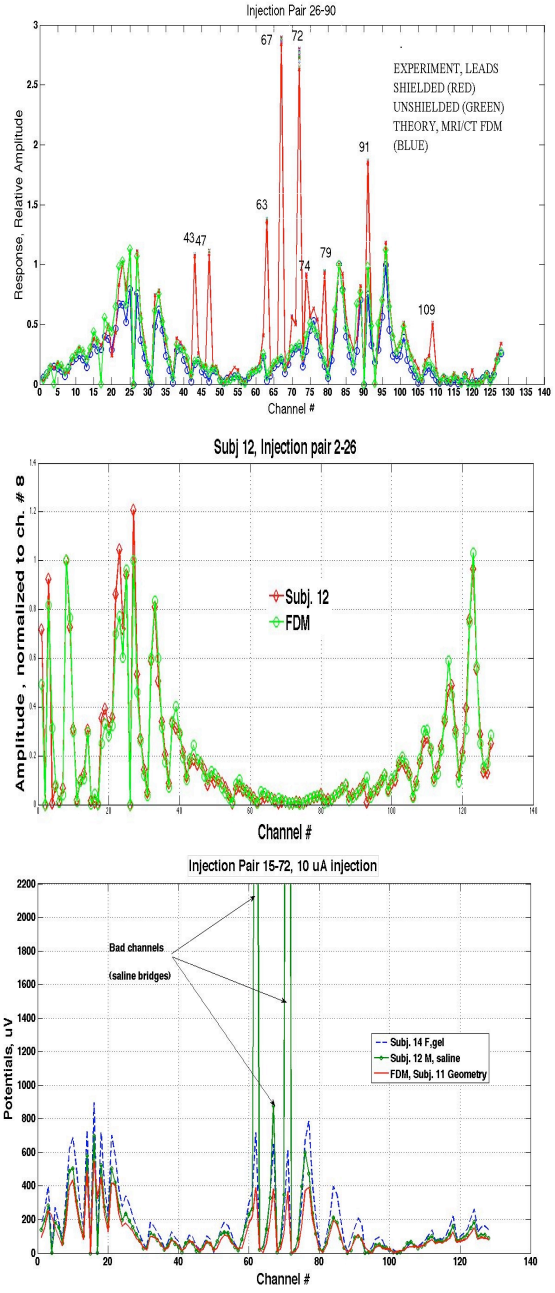

Figure 1. Potentials versus channel #. Top: Subject 11 data. Middle: Subject 12 data. Bottom: Female Subject 14 and male Subject 12 data compared with FDM of Subject 11. The major bad channels are marked in the graphs.

After correcting the flaws in our initial current injector design and extensive tests with a test fixture (i.e. resistor ladder) and saline head phantoms, we resumed the human subject experiments. The expected topography had been precalculated with Subject 11's head model for the injection configuration used afterwards in experiments. In this *a priori* simulation the conductivities values or the head tissue compartments had been taken from most recent literature [14]: (scalp – 0.44S/m, brain – 0.25 S/m, CSF – 1.8 S/m, and skull – 0.018 S/m). The initial experiments were done with saline electrolyte and shielded leads nets. In Figure 1 we present the results of successive experimental protocol improvements. Typical results comparing the potentials on the head of Subject 11 (bald, no hair) measured in bEIT with shielded and unshielded leads are presented in the top graph. One can see that in the case of unshielded leads the agreement with simulation is very good and the problem of bad channels is reduced. Channels # 4 and 93 are zeroed due to the EEG amplifier circuitry, and channel # 17 in the unshielded net had permanently damaged insulation. These bad channels were identified prior to the experiment by a routine gain and impedance check. We believe that in the shielded case most likely the bad channels are due to unpredictable moisture shorting the electrodes and shields between passive and active channels via the amplifier common, as described earlier. After this experiment and later on we were using only unshielded nets.

In the middle of the Figure 1 one can see excellent agreement of the measured and predicted topographies for the forehead area (channel pair 2-26) where there was no hair issue (Subject 12, thick hair). However, as we expected there were about 8 saline "bridges" around the active channel # 90 which were picking-up its high potential for the injection pair 26-90 (see Figure 1, bottom). In this case channel # 26 is the same forehead channel and it is good, while channel # 90 is in a thick hair area which causes numerous saline bridges in its vicinity (the nearest neighbors: channels # 77, 83, 84, 85, 89, 91, 95). Similar bridging with Subject 12 was observed in all cases when the active electrode was positioned in a region of hair, while no such issues arose for Subject 11. After observing this trend, we realized that a saline bridge issue existed for thick hair leading to high voltage readings in the immediate neighborhood of the active channel, but those could be avoided using gel electrolyte or by careful *a posteriori* elimination. Therefore, in the experiments with female Subjects 14 and 15, we used only gel electrolyte and unshielded nets. This modification addressed the problem of saline bridges effectively as can be seen in the bottom graph of Figure 1 for Subject 14 (female, thick hair) in comparison with data for Subject 12 (male, saline net, thick hair).

For Subject 14, there were no new bad channels besides identified earlier in the amp circuitry (channels

4 and 93) and net wire (channel # 17). Potentials are plotted as they measured and calculated in the model in micro-volts. The theoretical curve (red) is in a good agreement, though, it was not expected to match the experiment perfectly as it was calculated on the basis of different geometry (Subject 11) with 2 mm

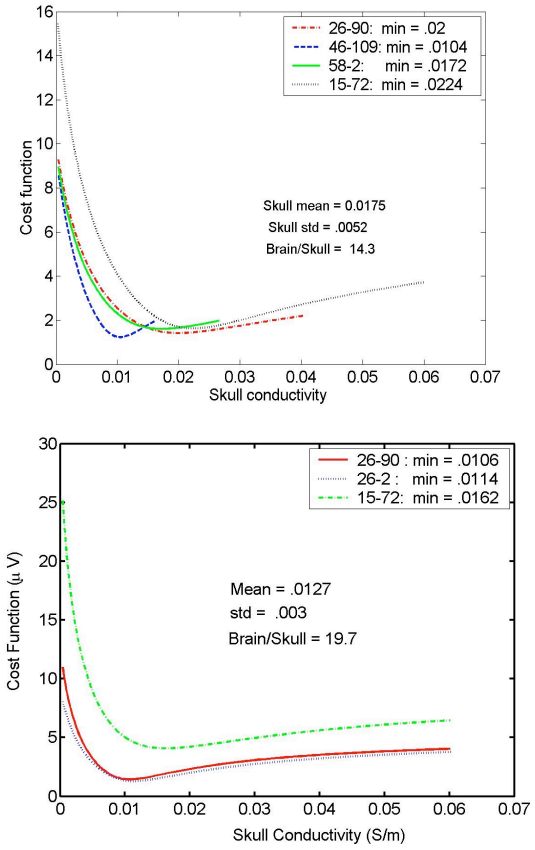

Figure 2. The cost function minimization for Subject 11 (top) and Subject 12 (bottom) for different skull conductivities when the rest of the tissue conductivities are fixed to their best estimates. Injections pairs and the skull conductivities minimizing the cost function are shown in the legends. These results proves 1:15 ratio of skull to brain conductivity rather than 1:80 [27]. Resolution is 1 mm.

resolution and given for a typical conductivity parameters set from recent literature without any additional fitting. Taking into account the good fit to the experiment seen in Figure 1, we can conclude that we have measured the skull to brain conductivity ratio roughly as 1:15 which agrees with the most recent results of other groups [8], [10], [29], [30].

Before applying the inverse solver we decided to tune our estimates in 1D by alternatively varying the conductivity of a tissue of interest and fixing the rest of the tissue conductivities at the best previous estimates. The results of such a search are shown in Figure 2 and 3. We have started from the set of conductivities used to match the patterns in Figure 1. First we dealt with the most important skull conductivity fitting, as the skull data reported in the literature have the largest uncertainty: the variations reported reach up to 1000% [31]. We have processed so far only data from a few injection pairs for Subjects 11 and 12; the results are summarized in Figure 2. One can see that the skull conductivity estimate for the sagittal injection pair 15-72 (where the bones are thick) is larger in both cases (Caucasian and Asian adult male), while also slightly higher (0.022 versus 0.016 S/m) for the Caucasian subject. At the same time the transverse injection pairs (109-46 and 26-2) produce smaller estimates 0.010 and 0.011 respectively. These results are in good agreement with the findings by Oostendorp et al. [8] who also used a similar technique and current injection pattern.

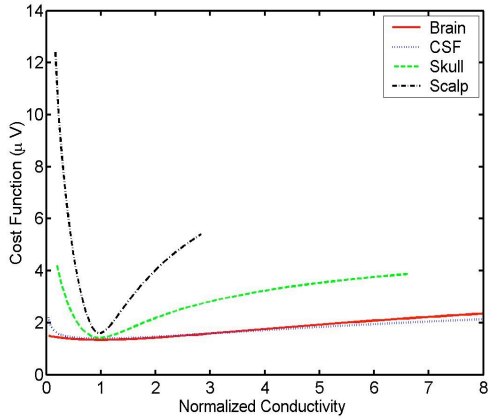

Figure 3. Cost function versus normalized tissue conductivities for Subject 11, injection pair 26-90, at 1 mm resolution. The cost function is most sensitive to the changes in scalp and skull, and less sensitive to CSF and brain conductivity changes.

One possible explanation for this result is that the front and rear skull regions are thicker (having a tri-layer structure with marrow [31]) whereas the temporal skull plates are compact, and resistive, cortical bones.

In Figure 3 we show cumulative behavior of the cost functions when all tissue conductivities are varied separately. Several important conclusions can be drawn from these results. It seems the forward solution for externally impressed current is more affected by the scalp and skull misspecifications in conductivities than by brain or CSF misspecifications. For instance, a 100% change in the scalp conductivity from the nominally true value will result in the error function change which is two times larger than the change

caused by the similar 100% change in the skull conductivity. At the same time, the cost function has almost a flat response to CSF and brain conductivity changes within the given scale. Nonetheless, when the scalp conductivity and skull conductivity are fixed near the minimum values, the brain and CSF conductivities variation also generates pronounced minima, but at the lower scale of the cost function variability. That proves that one can measure the conductivity even for these intracranial tissues shielded by the skull. The result of such estimates is given in Table 1 for Subjects 11 and 12. Surprisingly, the conductivities extracted for Subject 11 for scalp, brain and CSF are very close to the average literature data. With the help of the inverse search engine applied at its full extent, we hope to further fine tune the estimation of these values.

4. Discussion

We have extracted major regional conductivity values for skull, scalp, brain, and CSF for two male adults (Caucasian and Asian descent) and also preliminarily showed that the collected data for the female subjects (both Caucasian) are in the appropriate physiological range [14]. Most importantly, we showed that the skull-to-brain conductivity ratio is 1:15 rather than 1:80 as it is believed in the mainstream literature [27]. We have upgraded our computational engine to treat inhomogeneity of the skull trough parcellation and by introducing the powerful simulated annealing optimizer in the inverse search, and demonstrated the feasibility of solving the problem for 12–20 unknowns (for synthetic data). Finally, we have designed, built and tested hardware and data acquisition software for bEIT and proved that the data collection is achievable in reasonable time and at an affordable cost, and computational post-processing is scalable in a multi-processor computational environment.

In general, we have found that the measurement patterns are pretty much robust with respect to subject variability which is typically not larger than 20–30% when the data of all subjects are superimposed on a single graph (not shown). We believe we are able to make estimates of individual's head tissue conductivities based on the atlas head, or any other realistic head geometry even without warping, as it will just compromise accuracy to some degree. The spatially resolved models of skull bones and the use of a 256-channel net with larger number of active interrogating pairs should increase the sensitivity of this method.

Overall, the collected experimental data are sound and prove our previous assumptions: there is a small phase shift on the active channels, mainly due to contact capacitance [28]. The phase is noisy, but improves significantly when increasing the level of injection from 5 μA to 40 μA. There was also a weak dependence of the measured bEIT topography on the driving frequency, but it should not be of immediate concern, as it was in the margin of other estimated errors. The more thorough analysis of the observed phenomena would require use of a complete EIT electrode model and taking into account distributed capacitance effects in the head tissues.

To make this technology work, it is important however to recognize and carefully remove the bad channel outliers. On the other hand, the active current injection-interrogation of the head and comparison against the pre-calculated pattern appears to be a good candidate for bad channel detection for other EEG applications too. It is much more sensitive in recognizing the shorted or saline-bridged channels than usual impedance measurements and bridge detection functions presently integrated into EEG control and analysis software.

5. References

[1] Lantz, G., R.G. de Peralta, L. Spinelli, M. Seeck, and C.M. Michel, "Epileptic source localization with high density EEG: how many electrodes are needed?", *Clinical Neurophysiology*, vol. 114, pp. 63–69, 2003.

[2] Wen, H., J. Shah, and R.S. Balaban, "Hall Effect Imaging", *IEEE Transactions on Biomedical Engineering*, vol. 45, pp. 119–124, 1998.

[3] Kwon, O., E.J. Woo, J.R. Yoon et al., "Magnetic resonance electrical impedance tomography (MREIT): simulation study of J-substitution algorithm", *IEEE Transactions on Biomedical Engineering*, vol. 49, pp. 160–167, 2002.

[4] Tuch, D.S., V.J. Wedeen, A.M. Dale et al., "Conductivity tensor mapping of the human brain using diffusion tensor MRI", *Proceedings of the National Academy of Sciences of the USA*, vol. 98, pp. 11697–11701, 2001.

[5] Huiskamp, G., M. Vroejenstijn, R. van Dijk, G. Wieneke, and A.C. van Huffelen, "The need for correct realistic geometry in the inverse EEG problem", *IEEE Transactions on Biomedical Engineering*, vol. 46, pp. 1281–1287, 1999.

[6] Holder, D.S., *Electrical Impedance Tomography*, Institute of Physics Publishing, Bristol and Philadelphia, 1st edition, 2005.

[7] De Munck, J.C., T.J.C. Faes, A.J. Hermans, and R.M. Heethaar, "A parametric method to resolve the ill-posed nature of the EIT reconstruction problem: A simulation study", *Annals of the New York Academy of Sciences*, vol. 873, pp. 440– 453, 1999

[8] Oostendorp, T.F., J. Delbeke, and D.F. Stegeman, "The conductivity of the human skull: Results of in vivo and in vitro measurements", *IEEE Transactions on Biomedical Engineering*, vol. 47, pp. 1487–1493, 2000.

[9] Van Burik, M.J., and M.J. Peters, "Estimation of the electric conductivity from scalp measurements: Feasibility and application to source localization", *Clinical Neurophysiology*, vol. 111, pp. 1514–1521, 2000.

[10] Gonçalves, S., J.C. de Munck, J.P.A. Verbunt, F. Bijma, R.M. Heethaar, and F.H. Lopes da Silva, "In vivo measurement of the brain and skull resistivities using an EIT-based method and realistic models for the head", *IEEE Transactions on Biomedical Engineering*, vol. 50, pp. 754–767, 2003.

[11] Wolters, C., "*Influence of Tissue Conductivity Inhomogeneity and Anisotropy on EEG and MEG based Source Localization in the Human Brain*", PhD thesis, University of Leipzig, 2003.

[12] Salman, A., S. Turovets, A. Malony, K.J. Eriksen, and D.M. Tucker, "*Computational modeling of human head conductivity*", Springer Lecture Notes in Computer Science 3514: Computational Science-ICCS 2005, V.S. Sundrem et al. (eds.), Springer-Verlag, pp. 631–638, 2005.

[13] Salman, A., S. Turovets, A. Malony, P. Poolman, C. Davey, K.J. Eriksen, and D.M. Tucker, "Noninvasive conductivity extraction for high-resolution EEG source localization", *Advances in Clinical Neuroscience and Rehabilitation*, vol. 6, pp. 27–28, 2006.

[14] Ferree, T.C., K.J. Eriksen, and D.M. Tucker, "Regional head tissue conductivity estimation for improved EEG analysis", *IEEE Transactions on Biomedical Engineering*, vol. 47, pp. 1584–1592, 2000.

[15] Salman, A., A. Malony, S. Turovets, and D. Tucker, "*Use of parallel simulated annealing for computational modeling of human head conductivity*", Springer Lecture Notes in Computer Science 4487: Computational Science-ICCS 2007, Y. Shi et al. (eds.), Springer-Verlag, pp. 86–93, 2007.

[16] Hoekema, R., G.J.M. Huiskamp, G.H. Wieneke, F.S.S. Leijten, C.W.M. van Veelen, P.C. van Rijen, and A.C. van Huffelen, "Measurement of the Conductivity of Skull, Temporarily Removed During Epilepsy Surgery", *Brain Topography*, vol. 16, pp. 29–38, 2003.

[17] Vauhkonen, P.J., M. Vauhkonen, T. Savolainen, and J.P. Kaipio, "Three-dimensional electrical impedance tomography based on the complete electrode method", *IEEE Transactions on Biomedical Engineering*, vol. 46, pp. 1150–1160, 1999.

[18] Vilhunen, T.,J., J.P. Kaipio, P.J. Vauhkonen, T. Savolainen, and M. Vauhkonen, "Simultaneous reconstruction of electrode contact impedances and internal electrical properties: I. Theory", *Measurement Science and Technology*, vol. 13, pp. 1848–1854, 2002.

[19] Ollikainen, J.O, M. Vauhkonen, P.A. Karjalainen, and J.P. Kaipio, "Effects of local skull inhomogeneities on EEG source estimation", *Medical Engineering and Physics*, vol. 21, pp. 143–154, 1999.

[20] Malmivuo, J.A., and V.E. Suihko, "Effect of skull resistivity on the spatial resolutions of EEG and MEG", *IEEE Transactions on Biomedical Engineering*, vol. 51, 1276–1280, 2004.

[21] Ross, A.S., G.J. Saulnier, J.C. Newell, and D. Isaacson, "Current source design for electrical impedance tomography", *Physiological Measurement*, vol. 24, pp. 509–516, 2003.

[22] Russell, G.S., K.J. Eriksen, P. Poolman, P. Luu, and D.M. Tucker, "Geodesic photogrammetry for localizing sensor positions in dense-array EEG", *Clinical Neurophysiology*, vol. 116, 1130–1140, 2005.

[23] Kromer, P., R. Robinett, R. Bengtson, and C. Hays, "PC-based digital lock-in detection of small signals in the presence of noise", *AAPT Apparatus Competition*, 1999.

[24] Poolman, P., R.M. Frank, and S.I. Turovets, "Modified lock-in detection for extraction of impressed EEG signals in low-frequency bounded-EIT studies of the human head", *International Conference on Image and Signal Processing (CISP 2008)*, accepted.

[25] Turovets, S., K. Glass, A. Malony, and V. Volkov, "*Finite Difference and Finite Element Human Head Modeling: Forward Problem*", Department of Defense, Telemedicine Advanced Technology Research Center (TATRC) Neuroinformatics Workshop, Eugene, OR, USA, 2003.

[26] Salman, A., S. Turovets, A. Malony, and V. Volkov, "Multi-cluster, Mix-mode Computational Modeling of Human Head Conductivity", *Proceedings of International Workshop on OpenMP* (IWOMP 2005), Eugene, OR, USA, 2005.

[27] Rush, S., and D.A. Driscoll, "Current distribution in the brain from surface electrodes", *Anesthesia Analgesia*, vol. 47, pp. 717–723, 1968.

[28] Schwan, H.P., "Electrode polarization impedance and measurements in biological materials", *Annals of the New York Academy of Sciences*, vol. 148, pp. 191–209, 1968.

[29] Clerc, M., G. Adde, J. Kybic, T. Papadopoulo, and J.M. Badier, "In vivo conductivity estimation with symmetric boundary elements", *Proceedings of the Joint Meeting of the 5th International Conference on Bioelectromagnetism and 5th International Symposium on Noninvasive Functional Source Imaging*, Minneapolis, USA, 2005.

[30] Zhang, Y., W. van Drongelen, and B. He, "Estimation of in-vivo brain-to-skull conductivity ratio in humans", *Applied Physics Letters*, vol. 89, pp. 223903-1–3, 2007.

[31] Law, S. K., "Thickness and resistivity variations over the upper surface of the human skull", Brain *Topography*, vol. 6, pp. 99–109, 1993. Rush, S., and D.A. Driscoll, "EEG electrode sensitivity - an application of reciprocity", *IEEE Transactions on Biomedical Engineering*, vol. 16, pp. 15–22, 1969